Stress-corrosion Cracking of Liquid-phase Sintered Tungsten Alloys

M. Z. SHAH KHAN*, J. H. UNDERWOOD** and I. A. BURCH*

*Materials Research Laboratory, Defence Science and Technology Organization, P.O. Box 50, Ascot Vale, Victoria, 3032, Australia

**Visiting Scientist from US Army Armament Research, Development and Engineering Center, Watervliet, NY 12189, USA

ABSTRACT

This study addresses the stress-corrosion cracking susceptibility of liquid-phase sintered tungsten alloys during long-term storage. These alloys are used for kinetic energy penetrators in military applications, and it is essential that the structural integrity of the penetrator does not diminish due to the combined action of chemical environment and residual manufacturing stresses.

The paper describes test methods used for assessing the resistance to stress-corrosion cracking in terms of the stress intensity parameter, K_{Iscc}. The alloys were obtained from different sources and had up to 10 weight per cent additions of selected combinations of Ni, Fe, Cu and Co, and different process variables. Cantilever bend specimens were used, and the test environment was an immersion in 3.5% NaCl aqueous solution followed by sustained loading in 95% relative humidity air.

The findings of this study were as follows: (a) Fracture mechanics was shown to give a good assessment and ranking of the resistance to stress-corrosion cracking of the various alloys. (b) The evidence of stress-corrosion cracking was found in the region controlled by stress intensity factor, generally designated as region III. (c) An unloading-compliance procedure similar to that applied in J-integral testing was shown to give accurate measurements of stress-corrosion crack growth. (d) A crack closure phenomenon was identified using the unloading-compliance procedure and attributed to the accumulation of corrosion products between the crack faces following certain times of exposure to the environment.

KEYWORDS

Stress-corrosion cracking, tungsten alloys, cantilever beam specimens, fracture mechanics, fracture modes, crack extension.

INTRODUCTION

Liquid-phase sintered tungsten alloys are produced by a powder metallurgical technique in which powders of W, Ni, Fe and Cu are compacted and then sintered at about 1400°C in a dry hydrogen atmosphere. The resulting alloys possess high strength and density, and their typical microstructure consists of rounded hard tungsten particles surrounded by a comparatively soft matrix phase (or binder) rich in the above elements.

Work in the past was directed towards improving the strength and ductility of sintered tungsten alloys by controlling their composition (O'Neil and Salyer, 1965; Churn and German, 1984) and processing (Edmonds and Jones, 1979; Kang *et al.*, 1981; Churn and Yoon, 1979; Muddle and Edmonds, 1980; German and Hanafee, 1982) such as rate of cooling from the sintering temperature. The stress-corrosion cracking susceptibility of high density liquid-phase sintered tungsten alloys has not been investigated extensively. In a recent study Chung and Duquette (1984) investigated two such alloys. In general, their study showed that a 90W-7Fe-3Ni alloy was susceptible to stress-corrosion cracking in a NaCl solution, while a 97WNiFeCuCo alloy was immune to such cracking after 200 hours of exposure. The current investigation addressed the stress-corrosion cracking susceptibility of sintered tungsten alloy systems during long-term storage. These alloys are used as long-rod kinetic energy penetrators in military applications, and it is essential that both the launch integrity and target-penetration capability of the penetrator does not diminish due to the combined action of sustained loading and chemical environment. Residual manufacturing stresses may be present in the penetrators, and exposure to saline environment is common during storage of naval munitions.

The approach taken was to study four alloys of various tungsten and binder composition, and determine their threshold stress intensities for stress-corrosion cracking (K_{Iscc}) by applying a fracture mechanics analysis. In addition to the determination of K_{Iscc} values, an unloading-compliance procedure was applied to measure crack growth under environmental conditions. The advantages of using the compliance procedure and the results will be discussed in the following sections. Using tensile test and indentation hardness data for one alloy system, a hardness-strength correlation was determined, and was utilised in estimating the ultimate tensile strength of the other three alloy systems. Detailed electron microprobe analyses were performed to obtain the chemical composition of the binder phase in each alloy system. The fracture surfaces were studied using scanning electron microscopy and the stress-corrosion fracture mechanism was described.

MATERIALS

Four tungsten based alloys were selected for this study, designated as 95WNiFe, 97WNiFeCuCo, 90WFeNi and 90WNiCu. Table I lists the nominal alloy compositions, and also the average compositions of the binder phase obtained from electron microprobe analyses. Microstructures of the alloys studied are shown in Fig. 1. Note that the tungsten particle size is clearly the largest in alloy 97WNiFeCuCo. The 90WNiCu alloy contained two binder phases as shown in Table I.

All tests on the above alloys were performed in the as-received condition. The post-sintering treatment for alloy 95WNiFe consisted of a vacuum anneal at 1100°C followed by rapid air cooling. Alloys 97WNiFeCuCo and 90WNiCu

were in the as-sintered condition. The post-sintering treatment for alloy 90WFeNi was a vacuum anneal at 1050°C for 1 hour then water quench, followed by a swaging operation of approximately 24% area reduction. Following swaging, alloy 90WFeNi was subjected to a heat treatment at 550°C for 1 hour, and then air cooled.

Table II lists the hardness and density for the alloys in the as-received condition. The table also includes the ultimate tensile strength and fracture toughness of the alloys; the procedures followed will be described in forthcoming sections.

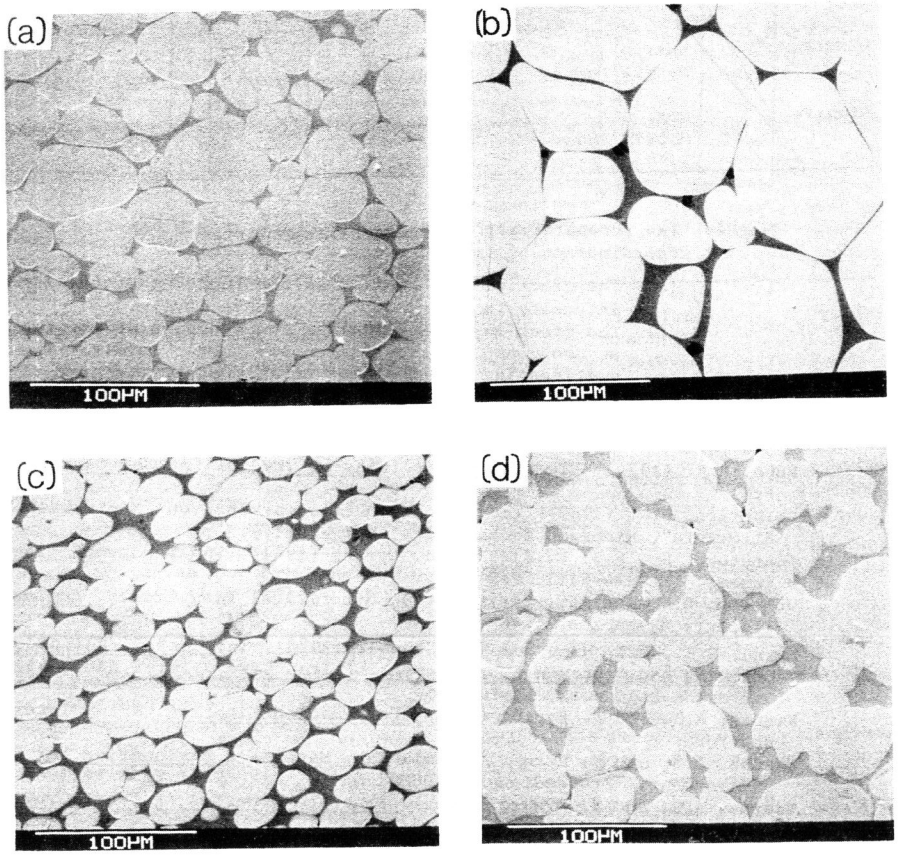

Fig. 1. Microstructure of the alloys investigated (a) 95WNiFe, (b) 97WNiFeCuCo, (c) 90WFeNi and (d) 90WNiCu. SEM photos of polished surfaces etched with Murakamis reagent.

Table 1. Material composition, weight percent.

ALLOY		W	Fe	Ni	Cu	Co
90WFeNi	Nominal	90.0	5.0	5.0	-	-
	Matrix Phase	23.0	38.3	38.7	-	-
90WNiCu	Nominal	90.0	-	7.5	2.5	-
	Matrix Phase-I	33.7	-	53.8	12.5	-
	Matrix Phase-II	2.4	-	38.4	59.3	-
97WNiFeCuCo	Nominal	97.0	0.7	1.6	0.5	0.1
	Matrix Phase	13.8	19.0	47.6	16.3	3.3
95WNiFe	Nominal	95.0	1.5	3.5	-	-
	Matrix Phase	26.2	21.0	52.5	-	-

Table II. Properties of the alloys investigated.

Alloy	Brinell Hardness Number, BHN	Density g/cm^3	Ultimate Tensile Strength, MPa	Fracture Toughness, $MPa\text{-}m^{1/2}$
95WNiFe	283	18.1	901 (a)	59.5 (c)
97WNiFeCuCo	285	18.5	908 (b)	49.5 (c)
90WFeNi	395	16.9	1258 (b)	54.5 (c)
90WNiCu	290	17.1	924 (b)	64.0 (c)

EXPERIMENTAL METHODS

Cantilever beam specimens were electric-discharge machined to the configuration shown in Fig. 2. Fatigue precracking was performed in three point bending with a cyclic frequency of 15 Hz using a MTS servo-hydraulic machine. As recommended by ASTM Standard E-399-81, the maximum stress intensity was kept below 60% of the K_{Ic} value in the final 2.5% portion of the crack length. The depth of the fatigue crack from the machined notch was such as to give a final a/W ratio of approximately 0.5. All precracking was conducted in a clean laboratory environment, 20 ± 2°C and 50% relative humidity.

(a) Determined from room temperature tensile tests.
(b) Determined using hardness/strength correlation.
(c) Determined by averaging K_{max} values obtained from three-point bend and cantilever-bend tests; only the toughness value for alloy 90WFeNi meets ASTM requirement (ASTM Standard E-399-81).

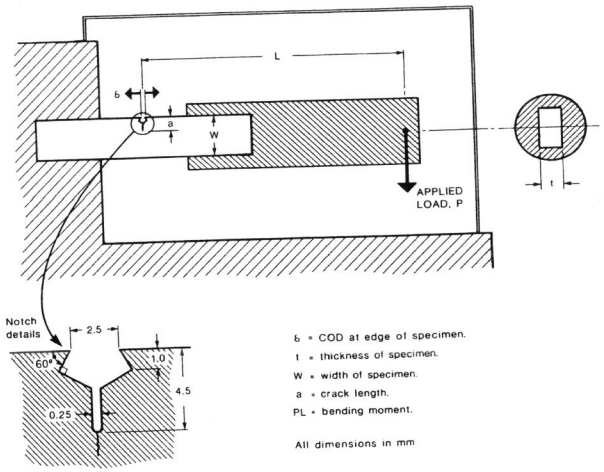

Fig. 2. Specimen details and test set-up for stress-corrosion cracking studies. Specimen thickness = 7.5 mm and width = 15 mm.

The stress-corrosion testing was performed in constant load cantilever bending as shown in Fig. 2. The relative humidity during the tests was maintained at 95 ± 1% by using a saturated aqueous solution of $CaSO_4.H_2O$ in containers placed inside an environment chamber. Both the temperature and humidity inside the environment chamber were monitored continuously during test.

The specimen for the tests was immersed in a 3.5% NaCl-distilled water solution for 1 hour, and following removal, left to dry in laboratory air for 24 hours. The specimen was then installed in the cantilever bend test set-up, and test loading commenced after the air inside the test chamber reached 95% relative humidity.

Individual specimens were loaded to preselected values. A clip gauge of the ASTM Standard E-399-81 type was mounted across the specimen notch and the crack opening displacement, δ, was monitored through a data acquisition system. The system consisted of a 20-channel amplifier receiving the clip gauge signal, an analog to digital converter and a printer which was programmed to print and record at pre-set time intervals.

An inverse form of the relation for δ in terms of a/W given by Tada *et al.* (1973) for pure bending was used to calculate a/W. This relation is

$$\frac{\delta BWE}{PL} = 24(a/W)\,[0.8 - 1.7(a/W) + 2.4\,(a/W)^2 + 0.66/(1-a/W)^2] \qquad (1)$$

for the range $0 < a/W < 1$

where

a/W = crack length to specimen width ratio
B = specimen thickness
PL = bending moment at the crack plane
E = Young's modulus.

Joyce *et al.* (1980) expressed the above relation in an inverse polynomial form which was further modified (Underwood *et al.*, 1987) for use here :

$$a/W = 1 - 3.83A - 1.81A^2 + 32.3A^3 - 44.2A^4 - 52.7A^5 \quad (2)$$

where $A = 1/[(\delta BWE/PL)^{1/2} + 1]$

for the range $0.3 < a/W < 1$

Using the crack length and the applied loads, the stress intensity, K, at the crack tip was evaluated from the expression described by Tada *et al.* (1973)

$$KBW^{3/2}/PL = 6\left(2\tan\frac{\pi}{2}\frac{a}{W}\right)^{1/2} \frac{(0.923 + 0.199\,(1-\sin\frac{\pi}{2}\frac{a}{W})^4}{\cos\frac{\pi}{2}\frac{a}{W}} \quad (3)$$

for the range $0 < a/w < 1$

In this study, the δ expression used, Eqn. 1, is for plane-stress conditions. The reason for this is that the δ measurements were at some distance away from the crack tip and therefore involve a large portion of the specimen. Plane-strain conditions dominate only very near the crack tip, whereas any displacement measurement away from the tip should be predominately plane-stress. From this reasoning, the critical values of K (K_{Ic} and K_{Iscc}) are plane-strain values, whereas the δ values are plane-stress. Later, it will be shown that a/W values calculated from δ (assuming plane-stress conditions) were in close agreement with those determined directly from fracture surfaces. An analogy can be found in Newman's (1974) work on the standard compact specimen. This author showed that δ measurements for a range of a/W ratios were bounded by the calculated δ values for plane-stress and plane-strain conditions. A closer observation showed that the δ measurements at and above a/W = 0.5 were in much closer agreement with the plane-stress calculations than with plane-strain.

RESULTS AND DISCUSSION

Strength and Toughness

The complex chemistry and structure of the liquid-phase sintered tungsten alloys can lead to difficulty in understanding the resultant mechanical properties. For example, in Table II, there is no significant difference in the as-received composite hardness with variations in tungsten particle size, tungsten composition and matrix phase elements (c.f. alloys 95WNiFe, 97WNiFeCuCo and 90WNiCu). Considering the as-received condition of alloy 90WFeNi, it appears that an increase in hardness and strength can be

achieved by a post sintering mechanical operation such as swaging. This increase in composite hardness is associated with the deformation and resulting hardening of the matrix structure.

Analysis of the tensile test data and Brinell hardness (ASTM Standard E-10-78) measurements on alloy 95WNiFe was performed in order to obtain a correlation between ultimate tensile strength and hardness. Using the ultimate tensile strength of 901 MPa (92Kgf/mm^2) and hardness of 283HB (Kgf/mm^2) for alloy 95WNiFe the following hardness to strength correlation was obtained :

$$\sigma_{uts} = 0.325\ HB \quad (4)$$

The determination of σ_{uts} for the other three alloys was carried out using the above correlation and their respective hardness values.

The fracture toughness of the alloys was determined using both three-point-bend and cantilever-bend tests. The toughness values reported in Table II are average K_{max} values obtained from one of each type of test. Figure 3 shows the results from cantilever-bend tests in terms of applied stress intensity, K_{appl}, as a function of δ. One alloy, 90WFeNi, was found to meet the specimen size requirement for plane-strain fracture toughness (ASTM Standard E-399-81). For other alloys the fracture toughness values in Table II may be higher than the actual values, perhaps by about 5%.

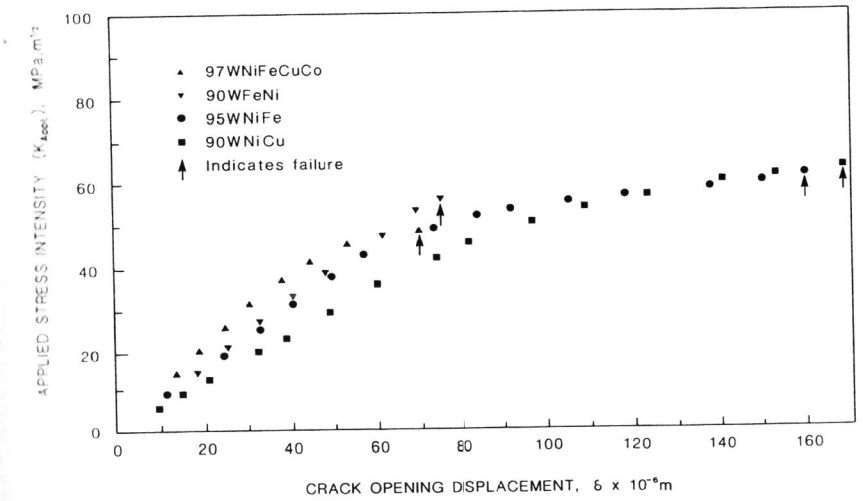

Fig. 3. Response of notched alloy bars in cantilever-bend tests.

The results show the loss in fracture toughness as the binder content decreases (c.f. alloys 97WNiFeCuCo, 95WNiFe and 90WNiCu); even a post-sintering mechanical treatment did not appear to cause as significant a loss in toughness as that associated with a reduced binder content (c.f. alloys 97WNiFeCuCo and 90WFeNi).

Fractography

Fractures in Fatigue and Bending Overload. Examination of the fatigue precrack region of the fracture surfaces showed the characteristic fatigue striations in the binder, areas of tungsten-tungsten separation, and areas of tungsten cleavage. Areas of tungsten-binder separation were also seen in alloy 97WNiFeCuCo which had the lowest binder content. Figure 4 depicts the modes of fatigue crack growth as mentioned above.

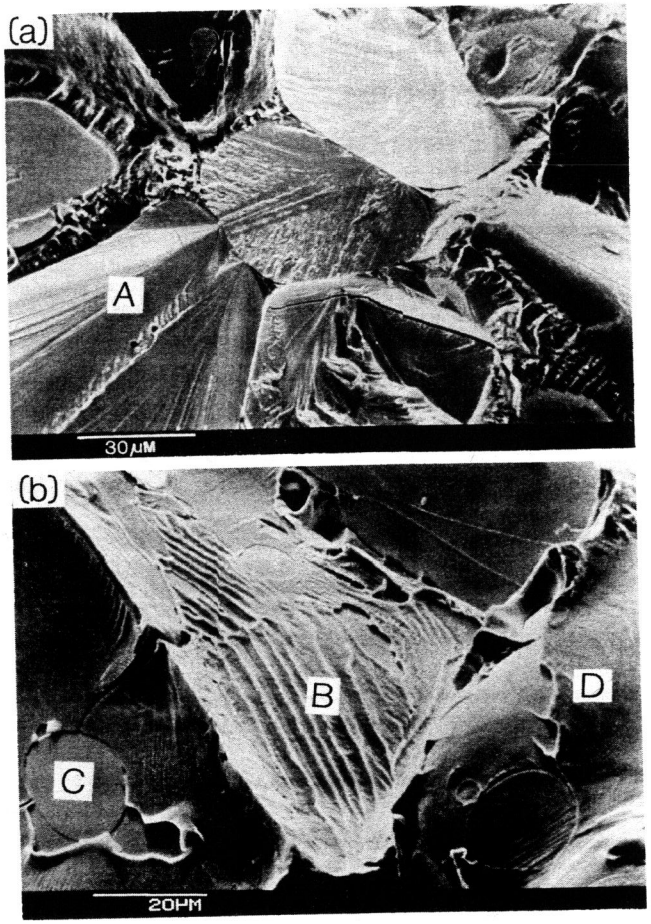

Fig. 4. SEM fractographs illustrating modes of failure under fatigue loading; tungsten particle cleavage (A), fatigue striations in the binder (B) tungsten-tungsten separation (C) and tungsten-binder separation (D). (a) Alloy 95WNiFe and (b) Alloy 97WNiFeCuCo.

The fracture surface in the bending overload region for alloys having 10% and 5% binder consisted primarily of binder failure by microvoid coalescence, cleavage of tungsten and tungsten-tungsten separation. In the case of alloy 97WNiFeCuCo, which had 3% binder, the overload fracture region consisted mainly of tungsten-binder separation, microvoid coalescence in the binder and tungsten-tungsten separation; cleavage of tungsten particles was negligible. Figure 5 shows the overload region with various modes of failure as mentioned above.

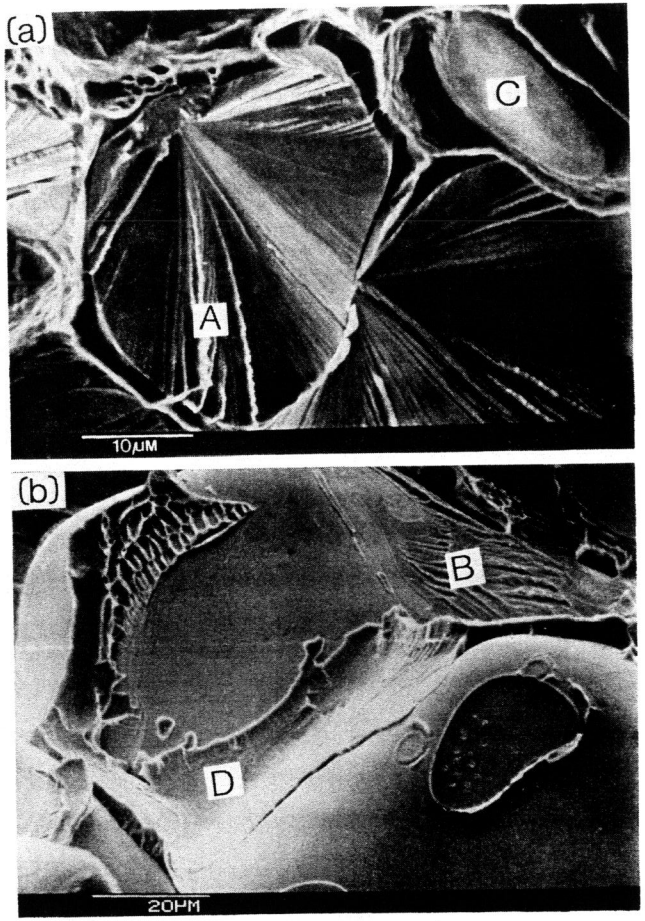

Fig. 5. SEM fractographs showing the various modes of failure in bending overload; tungsten particle cleavage (A), microvoid coalescence in the binder (B) tungsten-tungsten separation (C) and tungsten-binder separation (D); (a) Alloy 90WFeNi and (b) Alloy 97WNiFeCuCo.

Several investigations (Churn and German, 1984; Krock, 1966; Zukas, 1976) have identified similar failure modes in tungsten alloys. Generally, these studies showed that tungsten-binder separation, as seen in alloy 97WNiFeCuCo, tends to reduce the ductility of these alloys. The present study shows that tungsten particle cleavage is associated with the presence of two conditions. First, in order to bring about cleavage failure, a certain amount of particle-particle contact seems to be required. Second, the plane of the cleavage crack is typically observed to be at right angle to the particle-particle contact area. Figures 4a and 5a show examples of these features of the cleavage failure mechanism. Note the extension of cleavage fracture pattern from one particle to another over the contact boundary. In a situation where the crack plane lies approximately in the plane of the contact surface, then crack extension occurs by separation at the tungsten-tungsten interface.

Fracture under Stress-Corrosion. A knowledge of residual manufacturing stresses in these alloy systems is of great importance. If significant residual stresses are present, the long-term structural integrity of components could be affected. One way to observe their presence is to expose the alloys to the test environment free from externally applied stresses. In such conditions, cracking may occur if high enough tensile residual stresses are present in locations exposed to an aggressive environment. Such a study was conducted on 10 mm square polished specimens. After 500 hours exposure, isolated regions of the binder showed dissolution which resulted in the formation of mud-crack like pattern on the surface. These regions were numerous in alloy 90WNiCu while alloy 97WNiFeCuCo, having the lowest binder content, displayed fewer such regions. Alloys 90WFeNi and 95WNiFe were also found to be susceptible to such behaviour but to a much lesser extent. Figure 6 illustrates the regions where the above phenomenon occurred in the test environment. Chung and Duquette (1984) made similar observation in a 90WFeNi alloy and associate it with the presence of a brittle interphase

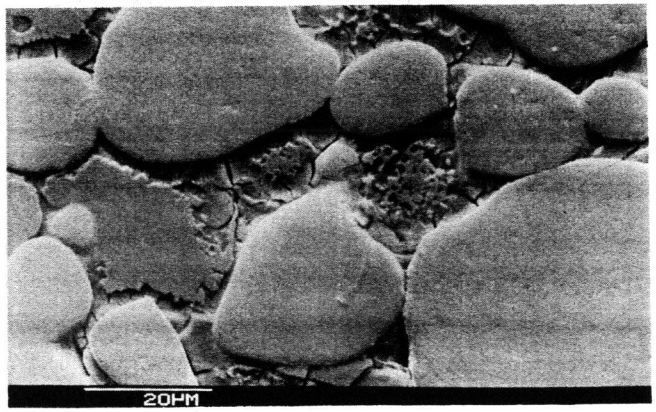

Fig. 6. SEM micrograph showing mud-crack like pattern in the binder after the polished specimen of alloy 90WNiCu was immersed in 3.5% NaCl solution and then exposed for 500 hrs in 95% R.H. with no external stress.

boundary precipitate. The existence of a brittle intermetallic phase was also identified previously by other workers (Edmonds and Jones, 1979; Muddle, 1984; Woodward *et al.*, 1985) in tungsten alloys. Optical metallography of sections beneath this product showed the absence of sub-surface cracks thus ruling out manufacturing residual stresses in the alloys as causing SCC.

The fracture surface of the specimens which failed under sustained external stress-corrosion displayed cleavage of tungsten particles, tungsten-tungsten particle separation and microvoid coalescence in the binder. As mentioned before, alloy 97WNiFeCuCo displayed, in addition to above failure modes, tungsten-binder separation. These failure modes, in combination with dissolution of the isolated regions of the binder, assisted in the overall crack growth. Figure 7 shows the SCC fracture surfaces with mud-crack like pattern clearly visible.

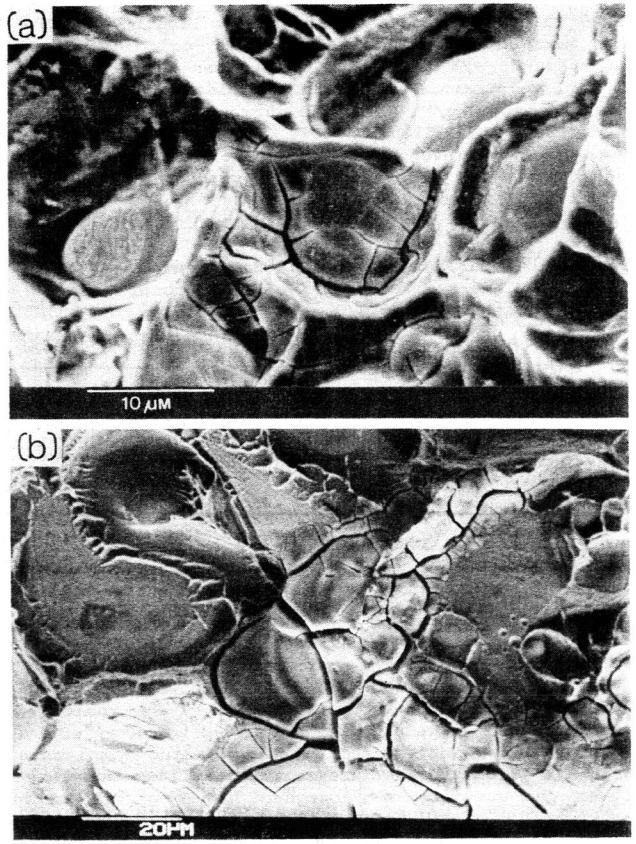

Fig. 7. SEM of SCC fracture surfaces (a) 90WFeNi and (b) 90WNiCu.

Unloading-Compliance Method

The concept of using a compliance technique to measure crack extension was first put forward by Irwin (1964). Later, Clarke *et al.* (1976) developed this technique and successfully applied it to single specimen crack extension measurement for J-integral fracture toughness testing. The unloading-compliance technique was found to be suitable in this present study for a number of reasons. First, the technique overcame the problems of mechanical and electrical drift commonly observed in long-term K_{Iscc} tests. Also, the technique gave measurements averaged over the whole crack front. Finally, the inherent difficulty in direct observation of stress-corrosion crack growth on the specimen surface was removed through the use of unloading-compliance.

Consider for example, alloy 90WFeNi, which was subjected to an applied stress intensity of 45.9 MPa.m$^{1/2}$ in the environment described previously. Table III compares the calculated plane-strain and plane-stress a/W values with the measured values of the fatigue precrack length from the fracture surface. The maximum difference between the calculated plane-stress values and the measured a/W values was less than 2%. For a similar comparison using plane-strain conditions, the disagreement widens between the calculated and measured a/W values, as shown in Table III. This shows that the plane-stress assumption is more appropriate for an unloading compliance procedure which involves a large portion of the specimen. In contrast, plane-strain conditions predominate very near the crack tip so that calculated stress intensities (ie K_{appl} and K_{Iscc}) are plane-strain quantities.

Table III. Comparison of calculated a/W under plane-stress and plane-strain conditions with measured a/W.

Calculated a/W		Measured a/W	Alloy
Plane Strain	Plane Stress	5-pt Average	
0.536	0.519	0.509	90WFeNi
0.533	0.517	0.507	90WNiCu
0.522	0.505	0.501	97WNiFeCuCo
0.525	0.508	0.504	95WNiFe

Another set of example results shows that stress-corrosion crack growth was conveniently monitored using the unloading-compliance procedure. Alloy 90WFeNi was subjected to an initial sustained stress intensity of 45.9 MPa.m$^{1/2}$ in the test environment. Table IV shows the calculated and measured crack growth in this particular test. As indicated in the footnote, the assumed Young's modulus was corrected to an effective modulus so that the calculated a/W (determined using unloading-compliance) agreed with the measured a/W (from the fracture surface) at time equals zero. This procedure improves the accuracy of subsequent crack growth calculations. Figure 8 shows a plot of a/W* versus time, where a/W* values were calculated using the effective modulus. Due to the difficulty in monitoring fast crack growth in the final stages, the last calculated a/W data point did not occur at the same time as the final failure.

Table IV. Calculated and measured crack length data for alloy 90WFeNi. E = 370,000 MPa; Effective Modulus, E* = 349,500 MPa. Failure Time = 92 hrs 46 mins.

Sustained Load Time Increment	δEBW/PL Unloading	a/W Calculated; Eq.1	a/W Measured; 5-point average	δE*BW/PL Unloading	a*/W Calculated; Eq.1
0	42.7	.519	.509	40.3	.509
1	43.8	.524	-	41.4	.515
2	46.8	.536	-	44.2	.526
3	51.3	.552	-	48.5	.542
4	53.7	.559	-	50.7	.550
5	64.4	.590	-	60.9	.581
6	-	-	.664	-	-

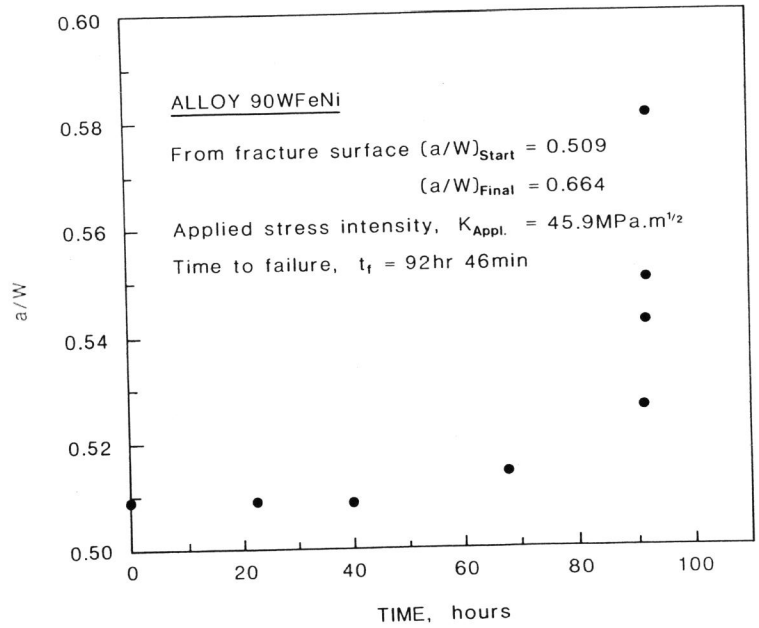

Fig. 8. Stress-corrosion crack extension as determined using unloading-compliance procedure. The data points correspond to the quantities in Table IV.

$$E^* = E \left[\frac{\delta EBW/PL \text{ measured; } t=o}{\delta EBW/PL \text{ calculated; } t=o} \right]$$

Unloading-compliance measurements were used to identify an apparent crack closure phenomenon during some of the K_{Iscc} tests. Typically, general corrosion was occurring, and the corrosion products were hindering the normal movement of the notch faces during the partial unloading/reloading exercise. This resulted in an apparent decrease in calculated a/W as a function of time.

Figure 9 illustrates the result corresponding to the crack closure phenomenon in terms of calculated a/W versus time. The alloy was 90WFeNi and was loaded to a stress intensity of 40.0 MPa.$m^{1/2}$, a value below the alloy's K_{Iscc}. The test was stopped after 500 hrs, and the corrosion products were cleansed from between the notch faces. Following this the specimen was loaded again to the stress intensity level initially used and an immediate unloading/reloading was performed to determine the a/W. As shown in Fig. 9, the value of a/W recovered approximately to the value obtained at the start of the test.

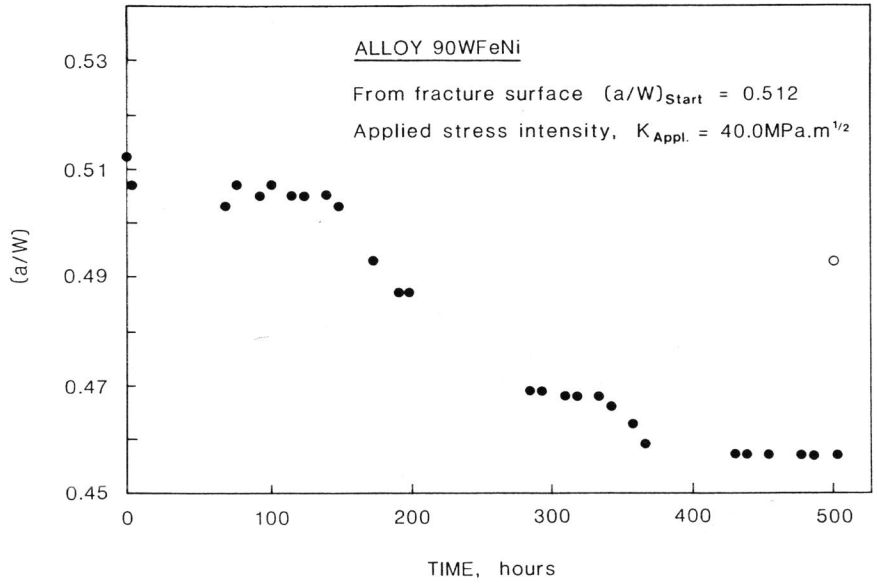

Fig. 9. Crack closure phenomenon as observed during SCC testing using unloading-compliance technique. The open circle corresponds to a/W obtained after cleaning off the corrosion products.

Similar apparent crack length reduction was observed by Joyce *et al.* (1980) working with depleted Uranium specimens. In their study the reduction in crack length occurred over the first 5 hrs of the test, and which resulted in specimen failure. The authors associated this behaviour to the presence of residual stresses and a plastic zone resulting from fatigue precracking. By contrast, in the present study, the apparent reduction in a/W was seen for an extended period in specimens which did not fail, and was due to the accumulation of corrosion products between the notch faces.

Stress-Corrosion Threshold

The resistance of materials to stress-corrosion cracking is measured in terms of a stress intensity threshold, designated as K_{Iscc} below which no crack extension occurs. Two approaches (Brown and Beachem, 1965; Speidel and Hyatt, 1972) have been used extensively in which specimens are loaded to various levels of stress intensities and either the crack velocity, da/dt, or the time to failure, t_f, is measured, as shown in Fig. 10 below.

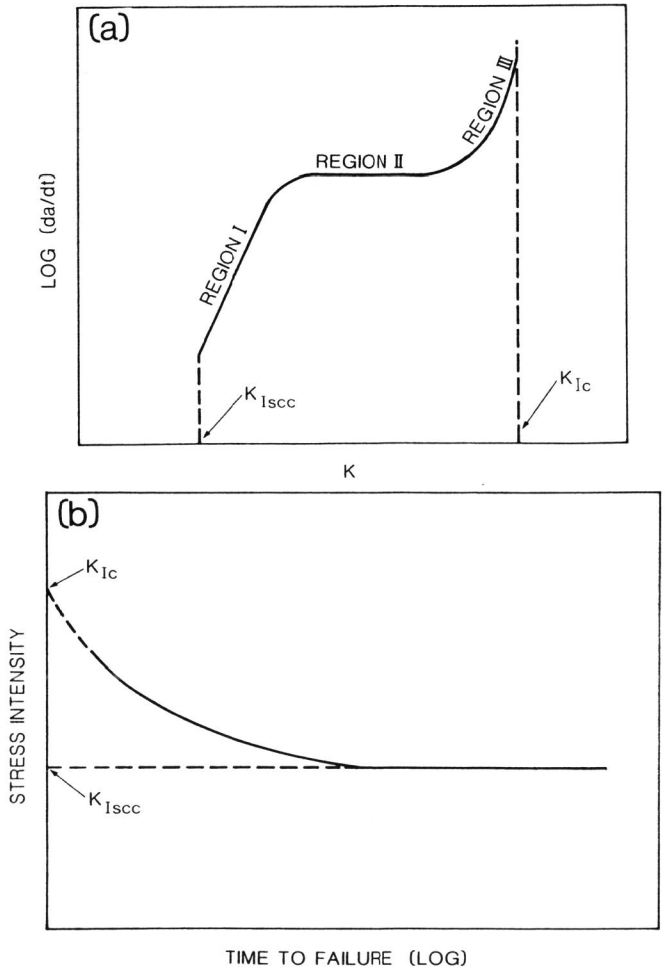

Fig. 10. Two approaches in determining K_{Iscc}; (a) da/dt versus K and (b) K versus t_f.

The da/dt versus K approach involves three regions with regions I and III being strongly stress dependent. The K_{Iscc} is obtained by extrapolating the lower end of region I to the abscissa. However, the measurement of K_{Iscc} using da/dt Vs K curve becomes difficult where the material behaviour does not show region I. In such a case the K_{Iscc} can be conveniently determined from K Vs t_f curve (Fig. 10b) by observing at what initial K level no failure occurs after a certain test duration, eg. 500 hrs.

In the alloys investigated here, the evidence of stress-corrosion cracking was found in the stress-intensity dependent region III. For this reason the ranking of the alloys according to their resistance to stress-corrosion cracking was accomplished by measuring K_{Iscc} from the K_{appl} Vs t_f curve. All the alloys showed susceptibility to stress-corrosion failure in an environment of 3.5% NaCl immersion followed by sustained loading in 95% relative humidity air.

Figure 11 illustrates the overall results in the form of K_{appl} versus t_f curves. These curves were extrapolated upwards to coincide with the respective alloys' fracture toughness, since the toughness is unlikely to be affected by environment in the fraction of a second required for fast failure. The threshold K_{Iscc} for the alloys varied from 32.6 MPa.$m^{1/2}$ for alloy 97WNiCuFeCo to 53.6 MPa.$m^{1/2}$ for alloy 95WFeNi. The K_{Iscc} was not a great deal different for the two 10% binder alloys, although the 90WNiCu alloy displayed a larger drop from its fracture toughness value to its K_{Iscc} value.

Alloy	Symbol	K_{MAX}	K_{ISCC} MPa-$m^{1/2}$
97WNiFeCuCo	●	49.5	32.6
95WNiFe	□	59.5	53.6
90WFeNi	△	54.5	45.2
90WNiCu	○	64.0	43.6

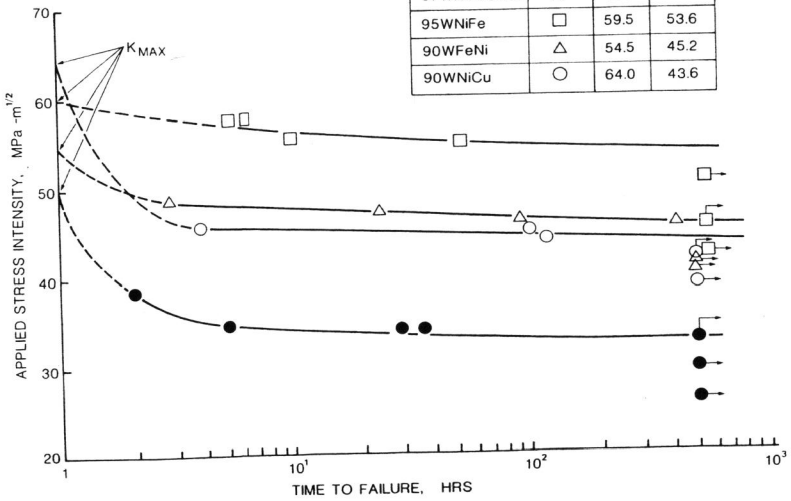

Fig. 11. Stress-corrosion cracking of W-alloys in terms of applied stress-intensity as a function of time to failure.

One of the alloys tested here, 97WNiCuFeCo, had the same composition as an alloy tested by Chung and Duquette (1984). Also, a similar environment was used, albeit in a different way. The K_{Iscc} results were quite different from that observed in the present study. The earlier work found no evidence of stress-corrosion cracking, whereas in the present work, K_{Iscc} = 32.6 MPa.$m^{1/2}$. This difference in K_{Iscc} results may be due to the difference in environment, exposure time and type of loading: the bolt-loading used in the earlier study involved a value of K_{Iscc} at about the level of K_{Ic}, which could cause extreme crack tip plasticity and so prevent or delay stress-corrosion cracking. The lower values in cantilever-loading, which established the K_{Iscc} in the present study, precluded any such overload.

The practical implication of the present study is that for tungsten alloy components subjected to significant levels of sustained tensile stress, including residual manufacturing stresses, storage should preclude chloride containing environments, especially marine, in order to extend their shelf-life and maintain their structural integrity in application.

CONCLUSIONS

The following conclusions were drawn from this study.

1. All the alloys investigated displayed susceptibility to stress-corrosion cracking in an environment of 3.5% NaCl immersion followed by sustained loading in 95% relative humidity air. Alloy 95WFeNi has shown the least susceptibility and narrowest range for SCC.

2 Fracture mechanics provided a quantitative assessment and ranking of the resistance to stress-corrosion cracking of the various alloys.

3 A variety of failure modes were observed in the alloy systems. The environment caused localized dissolution of binder regions and was responsible for crack growth under external sustained loads.

4 An unloading-compliance procedure similar to that applied in J-integral testing was shown to give accurate measurements of stress-corrosion crack growth.

5 A crack closure phenomenon was identified using the unloading-compliance procedure and attributed to the accumulation of corrosion products between the crack faces following certain times of exposure to the environment.

ACKNOWLEDGEMENTS

The authors are pleased to acknowledge J.C. Ritter and B. Hinton for helpful discussions in preparing this report.

REFERENCES

Brinell Hardness of Metallic Materials, *ASTM Standard* E-10-78.

Brown, B.F. and C.D. Beachem (1965). A study of the stress factor in corrosion cracking by use of the pre-cracked cantilever beam specimen. *Corrosion Science*, 5, 745-750.

Churn, K.S. and R.M. German (1984). Fracture behavior of W-Ni-Fe heavy alloys. *Metall. Trans.*, 15A, 331-338.

Churn, K.S. and D.N. Yoon (1979). Pore formation and its effect on mechanical properties in W-Ni-Fe heavy alloy. *Powder Met.*, 4, 175-178.

Chung, J.G. and D.J. Duquette (1984). Stress corrosion cracking behavior of tungsten heavy alloys. Materials Engineering Department, Rensselaer Polytechnic Institute, Troy, N.Y., Report # ARLCB-CR-84034.

Clarke, G.A., W.R. Andrews, P.C. Paris and D.W. Schmidt (1976). Single specimen tests for J_{Ic} determination. STP 590 ASTM, Philadelphia, 27-42.

Edmonds, D.V. and P.N. Jones (1979). Interfacial embrittlement in liquid-phase sintered tungsten heavy alloys. *Metall. Trans.*, 10A, 289-295.

Fatigue pre-cracking of K_{Ic} fracture toughness specimens, Annex A2, *ASTM Standard* E-399-81.

German, R.M. and J.E. Hanafee (1982). Liquid phase sintered W-Ni-Fe. In : *Processing of Metal and Ceramic Powders* (R.M. German and K.W. Lay, eds.), 267-282.

Irwin, G.R. (1964). Structural aspects of brittle fracture. *Appl. Mater. Res.*, 3, No. 2, 65-81.

Joyce, J.A., D.F. Hanson and C.R. Crowe (1980). Computer data acquisition monitoring of the stress corrosion cracking of depleted uranium cantilever beam specimens. *J. Testing and Evaluation*, 8, No. 6, 293-300.

Kang, T.K., E.T. Henig, W.A. Kaysser and G. Petzow (1981). Effect of cooling rate on the microstructures of a 90W-7Ni-3Fe heavy alloy. In : *Modern Developments in Powder Metallurgy* (H.H. Hausner, H.W. Antes and G.D. Smith, eds.), Vol. 14, 189-203.

Krock, R.H. (1966). Some comparisons between fiber-reinforced and continuous skeleton tungsten-copper composite materials. *J. Mater.*, Vol. 1, No. 2, 278-292.

Muddle, B.C. and D.V. Edmonds (1980). Interfacial segregation and embrittlement in liquid-phase sintered tungsten alloys. *Phil. Trans. R. Soc. Lond.*, A295, 129.

Muddle, B.C. (1984). Interphase boundary precipitation in liquid phase sintered W-Ni-Fe and W-Ni-Cu alloys. *Metall. Trans.*, 15A, 1089-1098.

Newman, Jr., J.C. (1974). Stress analysis of the compact specimen including the effects of pin loading. STP 560 ASTM, Philadelphia, 105-121.

O'Neil, J.W. and P.N. Salyer (1965). Massachusetts Institute of Technology - ASRL TR 132-2, Air Force Office of Scientific Research - AFOSR 66-1670.

Speidal, M.O. and M.V. Hyatt (1972). *Advances in Corrosion Science and Technology*, Vol. 2, 115-335, Plenum Press, New York.

Tada, H., P.C. Paris and G.R. Irwin (1973). *The Stress Analysis of Cracks Handbook*, Del Research Corporation, Hellertown, PA.

Underwood, J.H., I.A. Burch and M.Z. Shah Khan (1987). Analysis of some fracture mechanics test procedures for defence research applications. DSTO-MRL Report (in press).

Woodward, R.L., N.J. Baldwin, I.A. Burch and B.J. Baxter (1984). Effect of strain rate on the flow stress of three liquid phase sintered tungsten alloys. *Metall. Trans.*, 16A, 2031-2037.

Zukas, E.G. (1975). Coating tungsten composites for improved low temperature ductility. *Metall. Trans.*, 7B, 49-54.